

Journal of Biomedical Optics

SPIEDigitalLibrary.org/jbo

Cardiac-phase filtering in intracardiac particle image velocimetry

R. Aidan Jamison
Andreas Fouras
Robert J. Bryson-Richardson

Cardiac-phase filtering in intracardiac particle image velocimetry

R. Aidan Jamison,^{a,b} Andreas Fouras,^{a,b} and Robert J. Bryson-Richardson^c

^aMonash University, Division of Biological Engineering, Wellington Road, Clayton, Victoria 3800, Australia

^bMonash University, Mechanical Engineering, Wellington Road, Clayton, Victoria 3800, Australia

^cMonash University, School of Biological Sciences, Wellington Road, Clayton, Victoria 3800, Australia

Abstract. The ability to accurately measure velocity within the embryonic zebrafish heart, at high spatial and temporal resolution, enables further insight into the effects of hemodynamics on heart development. Unfortunately, currently available techniques are unable to provide the required resolution, both spatial and temporal, for detailed analysis. Advances in imaging hardware are allowing bright field imaging combined with particle image velocimetry to become a viable technique for the broader community at the required spatial and temporal resolutions. While bright field imaging offers the necessary temporal resolution, this approach introduces heart wall artifacts that interfere with accurate velocity measurement. This study presents a technique for cardiac-phase filtering of bright field images to remove the heart wall and improve velocimetry measurements. Velocity measurements were acquired for zebrafish embryos ranging from 3 to 6 days postfertilization. Removal of the heart wall was seen to correct a severe (3-fold) underestimation in velocity measurements obtained without filtering. Additionally, velocimetry measurements were used to quantitatively detect developmental changes in cardiac performance *in vivo*, investigating both changes in contractile period and maximum velocities present through the ventricular-bulbar valve. © 2012 Society of Photo-Optical Instrumentation Engineers (SPIE). [DOI: 10.1117/1.JBO.17.3.036007]

Keywords: filtering; image processing; velocimetry.

Paper 11510 received Sep. 15, 2011; revised manuscript received Dec. 5, 2011; accepted for publication Jan. 25, 2012; published online Mar. 23, 2012.

1 Introduction

The patterning of the embryonic heart is a complex process involving both genetic and environmental factors. Many of the genetic factors have been extensively studied and yet the role of environmental signals, including the flow of blood resulting from the heart's own pumping action, remains poorly understood. To examine cardiac hemodynamics *in vivo*, particle tracking and particle image velocimetry approaches have been developed that utilize a range of imaging modalities including confocal laser scanning microscopy,¹⁻³ ultrasound,⁴ and optical coherence tomography.⁵ The two major clinical techniques used for *in vivo* velocity measurements are magnetic resonance imaging (MRI) and ultrasound. Unfortunately, the near-wall resolutions of these modalities, 1000 to 1200 and 250 to 300 μm , respectively,⁶ are insufficient for high-resolution measurements in small vessels. Small animal versions of these systems are available for research purposes, with ultrasound systems being able to increase the spatial resolution of measurements at the expense of penetration^{7,8} and MRI systems attaining higher spatial resolution at the expense of temporal resolution.^{9,10} Laser Doppler is widely used for blood flow velocity measurements and relies on the optical Doppler effect of a frequency shift due to the movement of a scattering particle.¹¹ Additionally, laser speckle techniques have been used for flow measurements,¹² utilizing the alteration of speckle contrast due to particle movement to deduce that movement. A recent study has performed 3-D flow reconstruction using ultrasound

particle image velocimetry;¹³ however, the spatial resolution was an order of magnitude larger than that of the current study. More detailed reviews of all of these techniques can be found in Vennemann et al.¹⁴ and Fouras et al.¹⁵

Early work investigating the role of blood flow in the development of the heart has largely been carried out in the chick,^{8,16-18} utilizing the advantages of the external development of this system to allow physical manipulation. Work investigating blood flow has also been carried out in other species, such as the mouse^{19,20} and rat.^{21,22} A variety of surgical manipulations have been carried out on the developing chicken heart based on tying off arteries or veins, thereby altering the patterns of blood flow and increasing the pressure load on the heart. These studies have identified effects on the proliferation of myocytes,⁸ ventricular septal defects and semilunar valve malformations,¹⁶ as well as atrioventricular valve defects,¹⁷ together with a wide range of effects on chamber shape, stroke volume, heart rate, and cardiac output.¹⁸ Blood flow was assessed in these studies by the injection of dye into the bloodstream and video recording¹⁶ or by ultrasound echocardiography.⁸ In other cases, blood flow itself was not observed, but the resulting changes in morphology were examined. These studies clearly defined a role for blood flow in the patterning of the heart but were hampered by an inability to differentiate the effect of changes in blood flow from the longer term effects of increased cardiac pressure, together with difficulties in the detailed measurement of intracardiac blood flow caused by the high spatial and temporal resolutions required.

Research in the zebrafish model system has begun to remove these limitations and allow the detailed examination

Address all correspondence to: Robert J. Bryson-Richardson, Monash University, School of Biological Sciences, Wellington Road, Clayton, Victoria 3800, Australia. Tel: (+61) 3 9902 4629; E-mail: robert.bryson-richardson@monash.edu

of intracardiac blood flow. Zebrafish offer many advantages for the study of intracardiac flow, including the optical transparency of the early embryo, which allows the application of bright field imaging techniques for improved spatial and temporal resolution. Particle image velocimetry (PIV), an optical imaging method for measuring direction and velocity of flow patterns,²³ is ideal for *in vivo* whole-field blood velocity measurements. PIV requires a pair of images to be acquired at a specified time interval. Images are divided into interrogation windows and cross correlation used to determine the modal displacement of the window; this, combined with the known time interval, gives the instantaneous velocity. Microparticle image velocimetry (μ PIV), the application of PIV on a microscopic level, is a common variation of standard PIV, with its own advantages and disadvantages. For further details of the specifics of μ PIV, the reader is referred to Santiago et al.²⁴ Hove et al. were the first to exploit the transparency of zebrafish to conduct *in vivo* μ PIV and assessed the effect of intracardiac fluid forces on cardiogenesis.²

Because of the opacity of living tissue, *in vivo* PIV has only been conducted on a limited basis in small transparent vessels in rodents,^{25,26} chicken embryos,^{27–29} and zebrafish embryos.^{2,30} These studies have either injected tracer particles^{25,28–30} or used the red blood cells themselves as the tracer particles.^{2,26,27} Hove et al. applied PIV analysis to the heart using bright field imaging, using the red blood cells as tracers.² This method produces images in which the signal from the blood cells is contained within the same gray scale as other objects that are not of interest, for instance the heart wall. Because of the nature of PIV, both stationary and moving objects will contribute to the cross correlation and thus will impact the final velocity measurement. Hove et al. identified the presence of the heart wall and superficial tissue in their images as interfering with accurate velocity calculation, suggesting their velocity measurements represented an underestimation of the true value.² Lu et al. removed the impact of the wall by utilizing defocusing particle tracking velocimetry (PTV) on fluorescent tracer particles injected into the bloodstream, measuring velocity in three dimensions.³⁰ The use of fluorescent particles allows for the optical filtering of the contribution of the heart wall from the velocity calculation improving the accuracy of the flow measurements. However, as PTV requires the distance between tracer particles to be larger than their displacement, there is a severe limitation in the spatial

resolution of the technique, which provides only sparse instantaneous vector fields. Other studies in the zebrafish have utilized high-speed confocal or selective plane illumination microscopy of fluorescently labeled samples, together with the synchronization of confocal slices, to form dynamic 3-D models³¹ for examining the pumping mechanism of the embryonic heart,¹ and investigating valve formation.^{3,32} Despite the significant findings of these studies, the requirement for fluorescent imaging reduces the temporal resolution because of the longer integration times required.

The removal of stationary structures is common in methods such as *in vitro* X-ray velocimetry by removal of an average image composed by combining every image over the entire acquisition.³³ However, the dynamic nature of the heart makes subtracting an average image inappropriate. Cardiac-phase averaging, taking images at the same point in the cardiac cycle from successive heartbeats, has previously been utilized to improve signal-to-noise ratio in cardiac imaging by optical coherence tomography.⁵ Here we describe a cardiac-phase averaging method to remove the contribution of the heart wall and other interfering structures from bright field μ PIV analysis to improve the accuracy of blood flow measurements and allow the use of high-speed bright field imaging, providing improved temporal and spatial resolution. This technique has eliminated the severe underestimation of velocity measurements caused by the presence of stationary structures in μ PIV images, enabling accurate and quantitative detection of hemodynamic changes within the heart.

2 Results and Discussion

2.1 Image Acquisition and Phase Average Filtering

High-speed bright field imaging (2000 frames per second) was used to capture cardiac contraction over a 2-s window (approximately four cardiac cycles) in zebrafish ranging in age from 3 days post fertilization (dpf) to 6-dpf ($n = 4$ at each stage). Acquisition rates at this speed ensure that the desired pixel displacement is met for PIV analysis (1/4 of the interrogation window) at the high spatial resolution used in this study ($0.28 \mu\text{m}$ pixel size). At this rate of acquisition, we obtained ~ 800 instantaneous velocity measurement time points per cycle (depending on fish age).

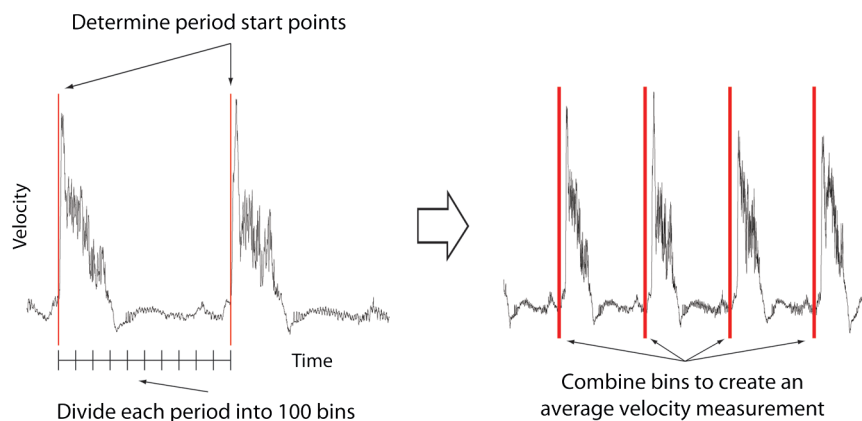


Fig. 1 Flow data is interrogated by performing PIV on a small section of the image to identify the start of each cardiac cycle. Each cardiac cycle is then divided into 100 bins. The velocity measurements from each bin in multiple cardiac cycles are combined to create a temporally averaged velocity measurement. For reference each cardiac cycle is approximately 800 frames in length.

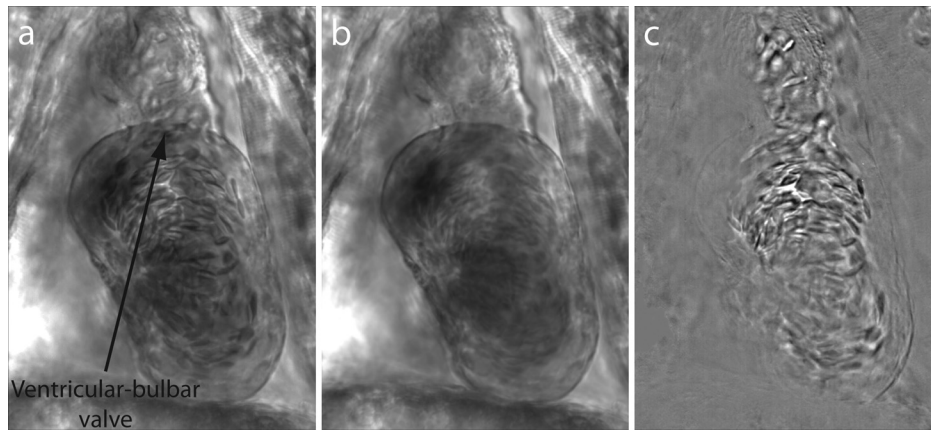


Fig. 2 Bright field microscopy images of a 4-dpf zebrafish heart. (a) Raw image of the zebrafish heart, (b) average image formed by the binning process described in Fig. 1, and (c) final image produced by subtracting the average image (b) from the raw image (a) (Video 1, QuickTime, 9.5 MB) [URL: <http://dx.doi.org/10.1117/1.JBO.17.3.036007.1>].

The temporal oversampling due to the high-speed acquisition of data can be used as an opportunity to improve the velocity measurements by binning the measurements into 100 sections in each cardiac cycle and averaging them to reduce erroneous vectors. Mathematical analysis of blood flow has successfully modeled cardiac output with a finite Fourier model having seven harmonics;³⁴ as a result, a minimum of 14 bins is required to accurately model cardiac function. Measurement-based studies have used larger numbers of bins to ensure the accuracy of results, for example, 42 bins per cardiac cycle, as used by Leo et al.³⁵ Cardiac defects may result in changes to the pattern of blood flow as well as the magnitude, resulting in a more complex model; therefore, we have utilized 100 bins in our analysis to ensure the accurate measurement of irregular flow patterns. Additionally, as each imaging sequence contains multiple cardiac cycles, it is possible to phase average the PIV measurements. These steps require first dividing each cycle into bins and then aligning the periods so that they are in phase with each other. By initially performing PIV on a small section of the overall image, the onset of contraction could be determined and used to align the cardiac cycles (Fig. 1). The binning of images from each cardiac cycle also removes the effect of variance in the length of each cardiac cycle (a variance of 10 to 15 ms being common). Each

frame within a cycle is allocated a relative bin within the cardiac cycle. This provides the ability to compare frames from different periods in this quasi-periodic flow, enhancing the accuracy of the velocity measurements acquired by reducing erroneous vectors. Because of the high temporal resolution of the acquisitions (~800 frames for one cardiac cycle of a 4-dpf embryo), each of the 100 bins contains approximately eight averaged velocity measurements from each cycle.

To remove the contribution of the static heart structures from the PIV analysis of blood flow, which causes underestimation of velocity, averaged images are created for each of the 100 bins within a cycle. Each average image is subtracted from the individual frames within the bin, resulting in the filtering of the static heart structures, and those moving less than 0.07 mm/s (which would appear stationary at these frame rates) are also removed from the imaging sequence as illustrated in Fig. 2 (Video 1). Following filtering, PIV analysis, using the full temporal resolution available, is carried out on the unbinned filtered images.

2.2 Particle Image Velocimetry Analysis

The computational expense of PIV can be reduced by defining the region of interest within the images for analysis. We carried

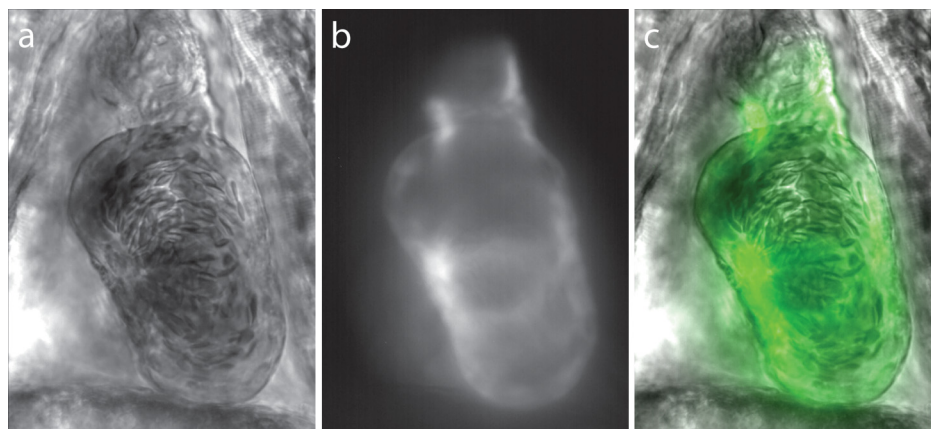


Fig. 3 Synchronization of bright field and fluorescent images for PIV mask creation. (a) Bright field microscopy image, (b) fluorescence image used for mask creation, and (c) combination of the two images following temporal alignment. The fluorescence image is seen to clearly identify the area of interest for velocity calculation.

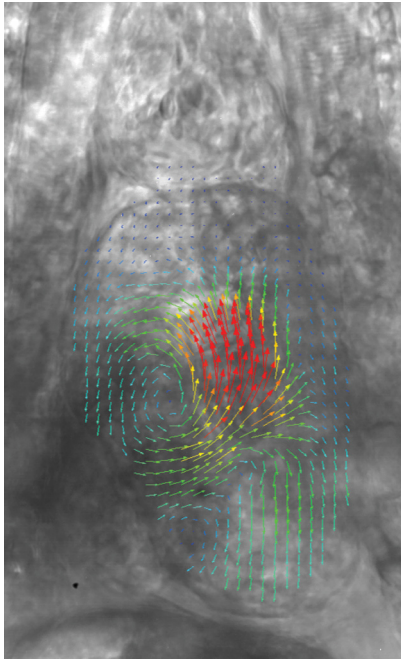


Fig. 4 Blood flow velocity measurements in a 6-dpf zebrafish during peak flow from the atrium into the ventricle. Vectors show direction and magnitude of velocity (standard color rainbow, red is high). Vectors are evaluated at $4.5\text{-}\mu\text{m}$ spacing with an interrogation window size of $18 \times 18\ \mu\text{m}$. For clarity only every second vector is shown. [Video 2](#) provides all 100 time-point measurements (QuickTime, 11.2 MB) [URL: <http://dx.doi.org/10.1117/1.JBO.17.3.036007.2>].

out imaging on zebrafish expressing green fluorescent protein under the control of the *cardiac myosin light chain 2* promoter. For each bright field acquisition, we captured a corresponding sequence of fluorescent images at a rate of 100 frames per second immediately following bright field capture. These fluorescent images were manually phase matched to the bright field images in order to provide a synchronized data set (Fig. 3) and thresholded to create a mask for the PIV analysis. The fluorescence image clearly identifies the area of interest for velocity calculation and is ideal for masking of the bright field images. The mask images were used to restrict the area of the image analyzed for PIV, reducing the computational expense of the technique. Additionally, by utilizing a mask we immediately combine heart wall information obtained from fluorescence imaging with the velocity measurements obtained from bright field imaging.

PIV analysis was carried out on each of the masked data sets to provide detailed velocity measurements over the period of

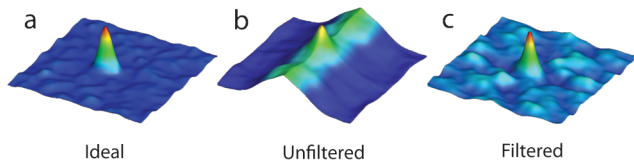


Fig. 5 Cross correlation images used in PIV analysis. (a) Cross correlation peak for synthetic, ideal data. (b) Cross correlation from 6-dpf unfiltered images. A clear ridge is evident distorting the peak, indicative of low-frequency noise such as stationary structures. (c) Filtering of the data analyzed in (b) demonstrating successful removal of noise from the analysis and improvement in the cross correlation, as evidenced by the similar appearance to the ideal case in (a).

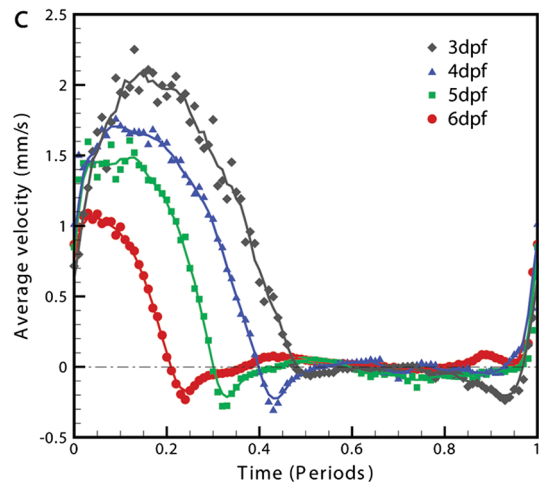
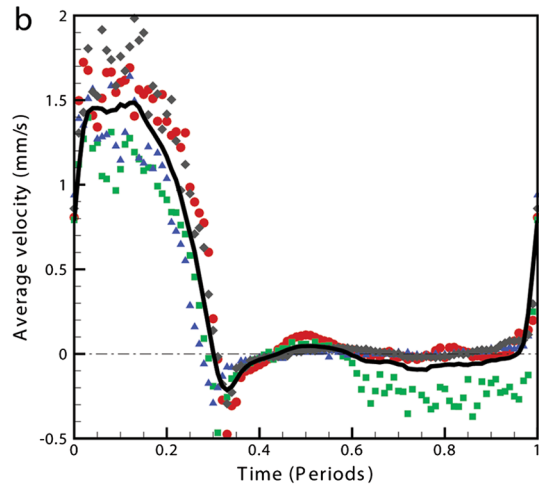
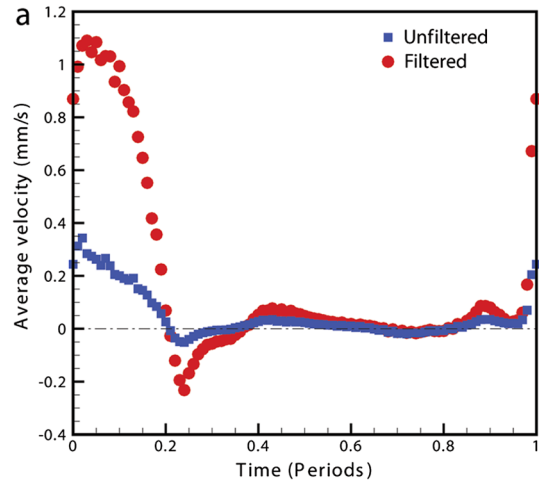


Fig. 6 Average velocity measurements through the ventricular-bulbar valve. (a) Comparison of velocity measurements before (blue squares) and after (red circles) cardiac-phase average filtering in a 6-dpf zebrafish. (b) Symbols provide velocity measurements for individual fish (red circles, green squares, blue triangles, and gray diamonds) at 5-dpf, and the solid line shows the average of these. [Video 3](#) provides the bright field imaging of the fish displaying retrograde flow through the ventricular-bulbar valve (green squares, QuickTime, 10.2 MB). (c) Average velocity measurements for each age group: 3-dpf (gray diamonds), 4-dpf (blue triangles), 5-dpf (green squares) and 6-dpf (red circles). Retrograde flow is evident in 3-dpf fish prior to systole between 0.8 and 1 period. ([Video 3](#), MOV, 9.7 MB) [URL: <http://dx.doi.org/10.1117/1.JBO.17.3.036007.3>]

zebrafish development from 3 to 6-dpf. Figure 4 (Video 2) shows the peak flow from the atrium to the ventricle and clearly illustrates the complexities of the flow being investigated. Video 2 illustrates the temporal resolution of the averaging technique, showing all 100 time-points (10 bins per second). These data show that for large parts of the cardiac cycle, the flow within the ventricle is negligible, with short periods of high inflow or outflow. Flow into the ventricle displays a vortical nature brought about by the enlargement of the chamber, while flow through the ventricular-bulbar valve is relatively parallel. Immediately after the valve the flow once again shows vortical nature owing to the expansion of the bulbus arteriosus.

To determine the improvement in PIV analysis following image filtering, we compared the cross correlation peaks obtained with and without cardiac-phase filtering to an idealized result generated with synthetic data (Fig. 5). Stationary structures within the image pairs will be included in the cross correlation, resulting in a shift of the apparent maximum of cross correlation towards the centroid of these structures and, in this instance, reducing the measured velocity. The noise resulting from these structures and the distortion of the cross correlation peak are clearly evident in the unfiltered data [Fig. 5(b)] but removed as a result of cardiac-phase filtering [Fig. 5(c)]. To examine the effect of cardiac-phase filtering on the velocity measurements, we compared the unfiltered data to the filtered data [Fig. 6(a)]. This comparison identified more than a 3-fold difference in average velocity during peak flow (1.1 mm/s in filtered data compared to 0.35 mm/s in the unfiltered data sets).

Within each age group filtered velocity measurements were highly reproducible and were used to form an average for each time point [Fig. 6(b)]. Figure 6(b) also shows the sensitivity of our approach. Note that Fig. 6(b) shows one fish exhibiting retrograde motion through the ventricular-bulbar valve in the latter part of the cycle. Remarkably, this retrograde flow, clearly evident in the quantitative analysis of this fish, can be seen to correspond to the leaking of one red blood cell (RBC) at a time back through the valve (Video 3).

Analysis of blood flow between 3 and 6-dpf identified a reduction in both peak velocity and the contractile period of the cardiac cycle as the fish increase in age [Fig. 6(c)]. The contractile period is seen to reduce approximately 10% each day between 3 and 6-dpf. Interestingly, this reduction in contractile period is not accounted for by a substantial change in heart rate (average 158 beats per minute). A steady decrease in the velocity is also witnessed during this age range [Fig. 7(a)]. Figure 7(b) provides the maximum velocity measurement recorded through the valve, rather than the spatial average used in Fig. 6, which nevertheless shows a similar trend to the spatially averaged results. This gives an indication of the maximum velocities measured in the center of the valve. We observe a high variance in maximum velocity between individuals, particularly in the younger age groups. Even within a single batch of fertilized embryos raised in the same conditions, there is subtle variation in the rate of development between individuals. We believe the high variance is due to these subtle variations in developmental rate as well as variation between individuals. The difference in development become less significant with time, and therefore there is decreasing variation with increasing age.

The measurements provided in Figs. 6 and 7 should not be confused with flow measurements or with oxygen transportation capacity. They represent the velocity at which the present RBCs are traveling. Two possible explanations for this reduction in both contractile time and velocity are the increase in size of the ventricular-bulbar valve and the increased hematocrit brought about by the ongoing production of RBCs during the early development of the embryonic zebrafish. These factors, individually or combined, may account for the reduction in velocity, while maintaining or increasing the fish's ability to circulate oxygen.

It is important that automated analyses of flow are able to detect subtle changes in heart function. One area of interest is the reverse flow through the valve. The motion witnessed in Fig. 6(c) immediately after systole in the 4-, 5-, and 6-dpf fish could easily be mistaken for retrograde flow through the

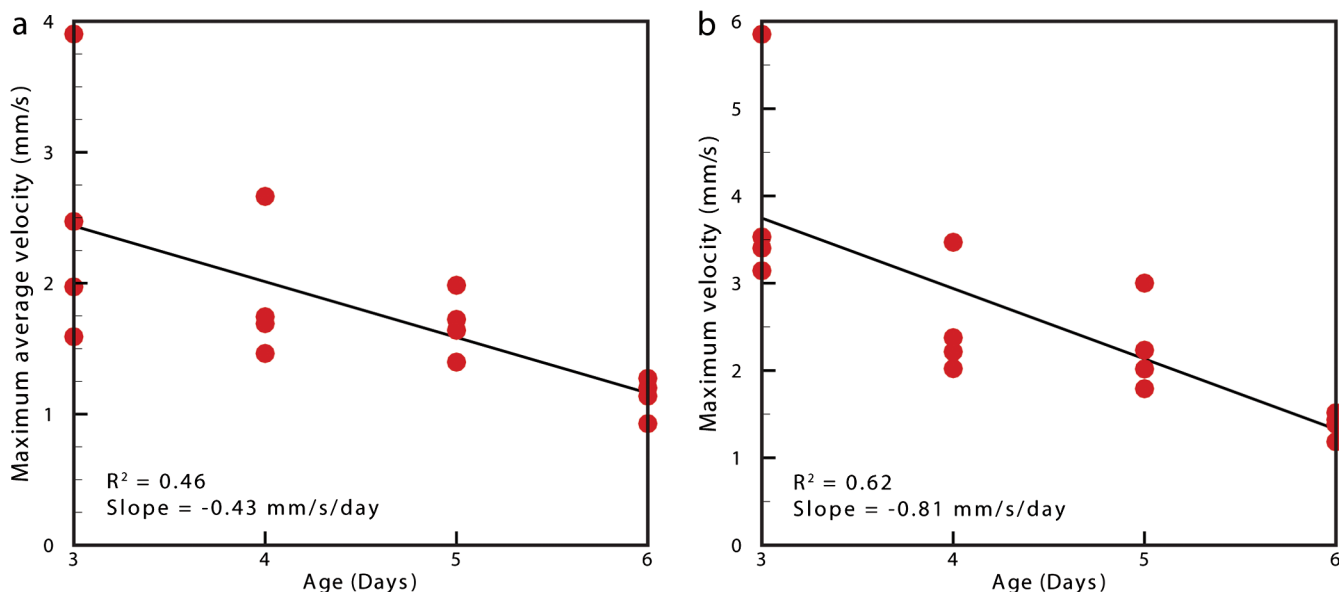


Fig. 7 Maximum average velocity (a) and maximum velocity (b) measurements acquired through the ventricular-bulbar valve. Maximum velocity and maximum average velocities are measured before and after spatial averaging is performed, respectively. Linear regression lines are provided for clarity.

valve; however, this motion is due to the closure of the valve pushing several RBCs back into the ventricle. While this trait is not present in the 3-dpf fish, reverse velocity measurements are evident immediately before systole. This motion is true retrograde flow caused by the force applied to the ventricular-bulbar valve as the ventricle expands. This force opens the underdeveloped valve, causing RBCs to move back into the ventricle through the ventricular-bulbar valve from the difference in pressure. These results demonstrate the capability of this approach to detect subtle developmental changes in the ventricular-bulbar valve.

3 Conclusions

A technique is presented for cardiac-phase filtering, demonstrating the adverse effect of the heart wall on velocity measurements obtained from bright field imaging. Removal of the heart wall was seen to result in the correction of a severe (3-fold) underestimation in velocity measurements. Additionally, the high spatial and temporal resolution used in this study was utilized to detect developmental changes within the embryonic heart. The contractile period of the heart was seen to significantly reduce as the fish increase in age (51% of the cardiac cycle for 3-dpf and 23% for 6-dpf), as measured by flow through the ventricular bulbar valve. Furthermore, the velocity through the valve was seen to also significantly decrease with age. Overall, this study demonstrates the ability of cardiac-phase filtering PIV to perform *in vivo* quantitative studies of developmental changes in the zebrafish heart.

4 Methods

4.1 Microparticle Image Velocimetry

An in-house code was used for performing the image processing and velocity measurements in this study.³⁶ This code has been developed over a number of years and rigorously validated by Fouras et al.³⁷ and Nesbitt et al.³⁸ Whole field velocity measurements were performed on the ventricle of each subject, which were masked by fluorescence image data. An interrogation window size of $18 \times 18 \mu\text{m}$ was used with a spacing between measurements of $4.5 \mu\text{m}$.

Velocity measurements through the ventricular-bulbar valve were calculated on a subregion of the full images $18 \times 18 \mu\text{m}$ in size (64×64 pixels). An initial large subregion of $45 \times 45 \mu\text{m}$ (160×160 pixels) was chosen so that the ventricular-bulbar valve was centered within the region. An interrogation window size of $18 \times 18 \mu\text{m}$ was used with a spacing between measurements of $2.25 \mu\text{m}$. The larger initial subregion ensures that RBCs in the desired subregion do not leave the image in the subsequent frame. The measurements outside the desired subregion are later discarded, and a spatial average of the remaining vectors is used to obtain the average velocity through the valve. Because of the small region size, no masking was used for these measurements.

4.2 Preparation of Zebrafish Samples

Homozygous transgenic *cardiac myosin light chain2-GFP* zebrafish embryos³⁹ were collected and raised in E3 embryo medium (50 mM NaCl, 1.67 mM KCl, 3.3 mM CaCl₂, 3.3 mM MgSO₄, in deionized water) at 28 °C. Embryos were anesthetized with 0.016% tricaine (3-amino benzoic acid ethyl ester) and mounted in 0.7% low-melting-point agarose dissolved in

E3 embryo medium together with 0.016% tricaine, prior to imaging. The embryos were mounted in Fluorodish imaging chambers (World precision instruments).

4.3 Imaging Setup

An inverted microscope (Leica DM ILM) with a 20× objective lens (Nikon bright field CFI Plan Apo 20 × /0.75) was coupled via an optical spacer (Leica 2.5×) to a high-speed camera (IDT Y4) to obtain an effective pixel size of $0.28 \mu\text{m}$. A three-axis robotic sample stage (Aerotech) was used for high-resolution (x, y resolution, $1 \mu\text{m}$; z resolution, $0.1 \mu\text{m}$) specimen positioning. Zebrafish with fluorescently labeled cardiac muscle cells were mounted such that viewing the heart was possible from below, enabling the main chambers of the heart to be in focus. Specimens were aligned to minimize flow in the out-of-plane direction through the ventricular-bulbar valve. Consistent orientation of the embryos was achieved by using the anatomical features surrounding the heart. Bright field imaging was used for PIV measurements, while fluorescence imaging was used to acquire heart wall information. The fluorescence images were acquired immediately after the bright field acquisition, with the only change to the optical path between the specimen and the camera being the inclusion of a dichroic filter. Temperature during image acquisition was 22.5 ± 0.5 °C.

Acknowledgments

We are grateful to Nick Lam for assistance with the *clmc2GFP* fish and to Monash Micro Imaging for the loan of filters for fluorescent imaging.

References

1. A. S. Forouhar et al., "The embryonic vertebrate heart tube is a dynamic suction pump," *Science* **312**(5774), 751–753 (2006).
2. J. R. Hove et al., "Intracardiac fluid forces are an essential epigenetic factor for embryonic cardiogenesis," *Nature* **421**(6919), 172–177 (2003).
3. J. Vermot et al., "Reversing blood flows act through *klf2a* to ensure normal valvulogenesis in the developing heart," *PLoS Biol.* **7**(11), e1000246 (2009).
4. B. C. W. Groenendijk et al., "The endothelin-1 pathway and the development of cardiovascular defects in the haemodynamically challenged chicken embryo," *J. Vasc. Res.* **45**(1), 54–68 (2008).
5. S. Bhat et al., "Multiple-cardiac-cycle noise reduction in dynamic optical coherence tomography of the embryonic heart and vasculature," *Opt. Lett.* **34**(23), 3704–3706 (2009).
6. R. S. Reneman, T. Arts, and A. P. G. Hoeks, "Wall shear stress—an important determinant of endothelial cell function and structure—in the arterial system *in vivo*," *J. Vasc. Res.* **43**(3), 251–269 (2006).
7. L. Sun, C. Lien, and K. K. Shung, "In vivo cardiac imaging of adult zebrafish using high frequency ultrasound (45–75 MHz)," *Ultrasound Med. Biol.* **34**(1), 31–39 (2008).
8. A. T. deAlmeida, T. McQuinn, and D. Sedmera, "Increased ventricular preload is compensated by myocyte proliferation in normal and hypoplastic fetal chick left ventricle," *Circ. Res.* **100**(9), 1363–1370 (2007).
9. H. Benveniste and S. Blackband, "MR microscopy and high resolution small animal MRI: applications in neuroscience research," *Prog. Neurobiol.* **67**(5), 393–420 (2002).
10. R. G. Wise et al., "Simultaneous measurement of blood and myocardial velocity in the rat heart by phase contrast MRI using sparse q-space sampling," *J. Magn. Reson. Imaging* **22**(5), 614–627 (2005).
11. A. Davis, J. Izatt, and F. Rothenberg, "Quantitative measurement of blood flow dynamics in embryonic vasculature using spectral Doppler velocimetry," *Anat. Rec.* **292**(3), 311–319 (2009).

12. S. Yuan et al., "Determination of optimal exposure time for imaging of blood flow changes with laser speckle contrast imaging," *Appl. Opt.* **44**(10), 1823–1830 (2005).
13. C. Poelma et al., "3D Flow reconstruction using ultrasound PIV," *Exp. Fluids* **50**(4), 777–785 (2011).
14. P. Vennemann, R. Lindken, and J. Westerweel, "In vivo whole-field blood velocity measurement techniques," *Exp. Fluids* **42**(4), 495–511 (2007).
15. A. Fouras et al., "The past, present and future of X-ray technology for in vivo imaging of function and form," *Appl. J. Phys.* **105**(10), 102009 (2009).
16. B. Hogers et al., "Extraembryonic venous obstructions lead to cardiovascular malformations and can be embryolethal," *Cardiovasc. Res.* **41**(1), 87–99 (1999).
17. D. Sedmera et al., "Remodeling of chick embryonic ventricular myoarchitecture under experimentally changed loading conditions," *Anat. Rec.* **254**(2), 238–252 (1999).
18. B. C. W. Groenendijk et al., "The role of shear stress on ET-1, KLF2, and NOS-3 expression in the developing cardiovascular system of chicken embryos in a venous ligation model," *Physiology* **22**(6), 380–389 (2007).
19. M. J. MacLennan and B. B. Keller, "Umbilical arterial blood flow in the mouse embryo during development and following acutely increased heart rate," *Ultrasound Med. Biol.* **25**(3), 361–370 (1999).
20. I. V. Larina et al., "Live imaging of blood flow in mammalian embryos using Doppler swept-source optical coherence tomography," *J. Biomed. Opt.* **13**(6), 060506 (2008).
21. L. Niu et al., "Ultrasonic particle image velocimetry for improved flow gradient imaging: algorithms, methodology and validation," *Phys. Med. Biol.* **55**(7), 2103–2120 (2010).
22. J. Jeong, Y. Sugii, and M. Minamiyama, "Measurement of RBC deformation and velocity in capillaries in vivo," *Microvasc. Res.* **71**(3), 212–217 (2006).
23. R. J. Adrian, "Particle-imaging techniques for experimental fluid-mechanics," *Annu. Rev. Fluid Mech.* **23**, 261–304 (1991).
24. J. G. Santiago et al., "A particle image velocimetry system for microfluidics," *Exp. Fluids* **25**(4), 316–319 (1998).
25. M. L. Smith et al., "Near-wall μ PIV reveals a hydrodynamically relevant endothelial surface layer in venules in vivo," *Biophys. J.* **85**(1), 637–645 (2003).
26. Y. Sugii, S. Nishio, and K. Okamoto, "In vivo PIV measurement of red blood cell velocity field in microvessels considering mesentery motion," *Physiol. Meas.* **23**(2), 403–416 (2002).
27. J. Y. Lee, H. S. Ji, and S. J. Lee, "Micro-PIV measurements of blood flow in extraembryonic blood vessels of chicken embryos," *Physiol. Meas.* **28**(10), 1149–1162 (2007).
28. C. Poelma et al., "In vivo blood flow and wall shear stress measurements in the vitelline network," *Exp. Fluids* **45**(4), 703–713 (2008).
29. P. Vennemann et al., "In vivo micro particle image velocimetry measurements of blood-plasma in the embryonic avian heart," *J. Biomech.* **39**(7), 1191–1200 (2006).
30. J. Lu et al., "Three-dimensional real-time imaging of cardiac cell motions in living embryos," *J. Biomed. Opt.* **13**(1), 014006 (2008).
31. M. Liebling et al., "Four-dimensional cardiac imaging in living embryos via postacquisition synchronization of nongated slice sequences," *J. Biomed. Opt.* **10**(5), 054001 (2005).
32. P. J. Scherz et al., "High-speed Imaging of developing heart valves reveals interplay of morphogenesis and function," *Development* **135**(6), 1179–87 (2008).
33. R. A. Jamison et al., "X-ray velocimetry and haemodynamic forces within a stenosed femoral model at physiological flow rates," *Ann. Biomed. Eng.* **39**(6), 1643–53 (2011).
34. S. A. Stevens, W. D. Lakin, and W. Goetz, "A differentiable, periodic function for pulsatile cardiac output based on heart rate and stroke volume," *Math. Biosci.* **182**, 201–211 (2003).
35. H. L. Leo et al., "Fluid dynamic assessment of three polymeric heart valves using particle image velocimetry," *Ann. Biomed. Eng.* **34**(6), 936–952 (2006).
36. A. Fouras, D. Lo Jacono, and K. Hourigan, "Target-free stereo PIV: a novel technique with inherent error estimation and improved accuracy," *Exp. Fluids* **44**(2), 317–329 (2008).
37. A. Fouras et al., "Volumetric correlation PIV: a new technique for 3D velocity vector field measurement," *Exp. Fluids* **47**(4), 569–577 (2009).
38. W. S. Nesbitt et al., "A shear gradient-dependent platelet aggregation mechanism drives thrombus formation," *Nat. Med.* **15**(6), 665–673 (2009).
39. C. J. Huang et al., "Germ-line transmission of a myocardium-specific GFP transgene reveals critical regulatory elements in the cardiac myosin light chain 2 promoter of zebrafish," *Dev. Dynam.* **228**(1), 30–40 (2003).